«ФИЗИКА ЭЛЕМЕНТАРНЫХ ЧАСТИЦ И АТОМНОГО ЯДРА»
1996, ТОМ 27, ВЫП.3

УДК 539.1.076 + 621.384.6

INNOVATIONS IN ACCELERATOR TECHNOLOGY

E. Tsyganov, A. Taratin, A. Zinchenko*

Joint Institute for Nuclear Research, Dubna, Russia

High energy particle colliders are probably the most sophisticated machines ever built. Colliding beams have to be kept stable for many hours, and beam parameters should be preserved for delivering maximal information to the physicists. Optimization of collider performance is a very important and challenging task, due to the complexity and required precision of experiments, as well as the high cost of the operating the accelerator complexes.

We review several promising directions for improvements in high energy collider performance that have been initiated and reported in scientific publications recently, namely: extraction by means of a crystal of the beam halo from high energy colliders for use in auxiliary experiments; compensation of mutual space charge effects of collider beams on one another; intelligent beam damping schemes and application of these to feedback systems; beam parameter diagnostics by use of low energy beam probes. To facilitate these developments an efficient software model of the collider was developed and applied to study details of the performance of the collider. A computer code for tracking charged particles in the collider environment was built, and some of its applications considered. All of these studies show promise of improving collider parameters and performance. Improvement of collider operations would extend the physics reach of existing and future colliding beam accelerators, and enhance the accessibility to scarce collider facilities for experimental groups.

Коллайдеры частиц высоких энергий являются, по-видимому, одними из наиболее сложных технических устройств. Ускоренные пучки частиц должны сохраняться в ускорителе в течение многих часов, причем их параметры должны оставаться стабильными, чтобы обеспечить получение максимума информации в экспериментальных исследованиях. Оптимизация работы коллайдеров является важной и очень непростой задачей из-за большой сложности и требуемой высокой точности экспериментов, а также высокой стоимости работы ускорительных комплексов.

*State University of New York at Albany, USA

Дается обзор нескольких перспективных направлений в усовершенствовании работы коллайдеров, которые недавно были инициированы нами и опубликованы в научных журналах и сообщениях, а именно: вывод гало пучка из коллайдеров частиц высоких энергий с помощью изогнутых кристаллов для организации дополнительных экспериментов на фиксированных мишенях; компенсация влияния пространственного заряда встречных пучков на их стабильность; новые схемы гашения колебаний пучка и их применения в системах обратной связи; неразрушающая диагностика параметров циркулирующих пучков с помощью пучков частиц низких энергий. Для детального исследования этих предложений нами была разработана эффективная компьютерная модель коллайдеров, созданы компьютерные программы для расчета траекторий заряженных частиц в кристалле, а также в поле пространственного заряда, электрических и магнитных полях в условиях, характерных для коллайдеров частиц высоких энергий. Результаты исследований дают основания надеяться на возможность значительного улучшения работы коллайдеров. Это позволит расширить область физических исследований, достижимых на сталкивающихся пучках существующих и сооружаемых ускорителей, и увеличит доступность этих ускорительных комплексов для большего числа исследовательских групп.

I. BEAM HALO CRYSTAL EXTRACTION DURING COLLIDING MODE

Bent crystals provide perhaps the only possibility to combine extraction of some fraction of the proton beam with colliding experiments. Studies on steering high energy beams using bent crystals and applications of this phenomenon for beam extraction have demonstrated the feasibility of this technique [1]. Figure 1 shows the results of the first experimental observation of the channeled particle deflection by a bent crystal at Dubna. Use of this technique could provide a double purpose mode of a collider operation, with extraction of a small fraction of beam intensity. This extraction may be performed with no interference with the colliding beam experiments.

Bent crystal extraction has been successfully demonstrated on almost all high energy accelerators [2,3,4,5]. Detailed studies of crystal extraction are in progress currently at Fermilab and CERN.

Despite success of beam extraction efforts, a practical solution for crystal extraction simultaneously with colliding beam experiments was not really found until recently. Early attempts to find the mechanism of «pumping out» particles from the primary beam and delivering them to the bent crystal without interference with beam emittance characteristics have been discussed [6,7] but not yet proved experimentally.

The matter of the high efficiency beam halo extraction from colliders during colliding mode of operation by means of a bent crystal was for the first time successfully elaborated by Monte Carlo simulation in the paper [8].

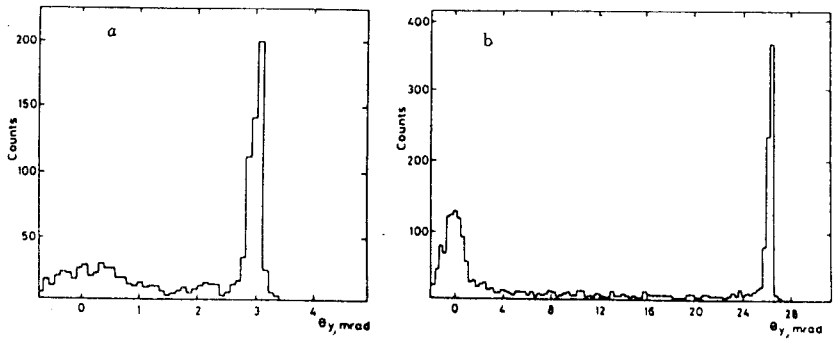

Fig.1. Angular distributions of the channeled fraction of 8.4 GeV protons outgoing from the bent crystal in the first experiment to observe bending in Dubna. For the crystal bending angle 3 mrad (*a*) and 26 mrad (*b*)

Calculations were performed for the Tevatron collider lattice. According to the studies [8] halo particles of high energy beams would be extracted from colliders with high efficiency without interference with colliding beam experiments. This would eliminate irradiation of accelerator parts by the beam halo, creating more favourable environmental situation at accelerators. The extracted beam could be used for parasitic experiments, or disposed of in an environmentally controlled manner.

The authors [8] have chosen the Tevatron lattice for the analysis because the Tevatron is the highest energy particle collider in the world today. Fermilab with rich infrastructure and scientific traditions in particle physics would be the natural center of activity of physicists in the near future, aiming also a preparation of elements of the LHC experimental detectors. Besides the rich expertise in colliding beam detectors, Fermilab could provide test beams of the highest energy. That is essential for a healthy R&D program in detectors for colliding beam experiments, especially for calorimetry. High energy particle beams at Fermilab should be considered as an essential contribution to the future LHC program.

Conventional extraction and colliding beam experiments are technically incompatible. Fermilab colliding beam program has an absolute priority, and therefore the fixed target mode of Tevatron operation is very strictly limited. Fermilab Main Injector extracted beam, 120 GeV, when it will be available, still cannot provide TeV beams for R&D in calorimetry.

The authors [8], based on the computer simulation, show how to extract 1 TeV beam halo protons from the Tevatron with high efficiency. More than 10^{-7} protons per second, now lost on scrapers and collimators, can be extracted

from Tevatron using bent crystal in a «passive» mode, without interference with colliding beam experiments. This would reduce background in the colliding beam detectors. The extraction efficiency can be as high as 99%. Bent crystal deflectors would also work well for the LHC collider, where background radiation due to a beam halo loss could be reduced by the factor of 100. The B-physics fixed-target experiments with the extracted LHC beam halo could be performed.

A. Resonance Excitation of Longitudinal Beam Halo. The main obstacle for crystal extraction is a very small impact parameter of a halo beam particle when it hits a bent crystal. Even if the crystal edge could be polished and aligned to the circulating beam with precision better than one micrometer, this effective septum thickness still is much larger than the typical impact parameter for a halo particle which impinges the crystal during beam loss, and therefore the septum cannot be effective. A small average impact parameter for particles striking the crystal could also worsen crystal radiation damage. For the device to be practical at least several micrometers are required for the mean impact parameter.

When one tries to excite beam halo particles using some kind of beam rf gimnastics and send them to the bent crystal septum [6], it is difficult to guarantee that the core of the beam is not disturbed and a beam emittance is preserved. Nevertheless, we showed by computer simulation [7] that perturbation pulses in the main rf voltage, if in resonance with the synchrotron oscillations of beam halo particles, can effectively eject the particles out of the bucket without perturbing the beam core. This method can be used to place the beam halo particles onto a bent crystal for extraction from an accelerator if the crystal will be located in high-dispersion region and thus particle momentum deviations can be translated into transverse displacements.

Suppose the driven halo particles are initially located in the δ–l phase space about (δ_p, l_p). Here $\delta = \Delta p / p_s$ is the relative momentum deviation from the synchronous momentum p_s, and l is the longitudinal displacement from the bunch center. Each time the driven halo particles complete one synchrotron oscillation, the perturbing pulses are switched on with the sign of δ_p. Thus the perturbed halo particles jump onto an orbit of larger amplitude after each synchrotron oscillation. Figure 2a illustrates the effect of one of the perturbing pulses in the δ–l space on the trajectory of the driven halo particle. The rf phase ϕ_p for the perturbing pulse is connected with l_p by the relationship

$$\phi = \phi_s + \frac{2\pi h}{C_s} l,$$

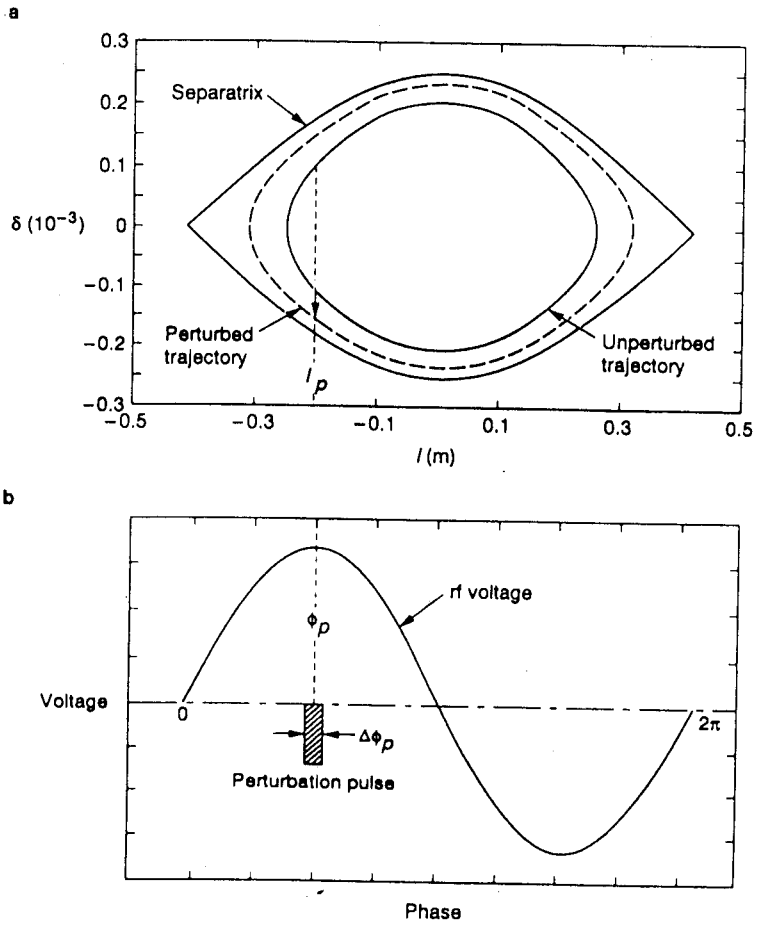

Fig.2. Schematic picture of the process of ejecting beam halo particles by means of synchronized rf voltage pulses. (*a*) Synchrotron orbits in the $\delta - l$ phase space before and after the action of a perturbation pulse. (*b*) Sinusoidal rf voltage and the position in rf phase of perturbation pulses

where ϕ_s is the synchronous phase, C_s is the circumference, and h is the harmonic number of the accelerator. The rf phase ϕ_p and interval $\Delta\phi_p$, in which the perturbing pulses are turned on are shown in Fig.2b. To act on halo particles only, the perturbing pulses, $\Delta\phi_p$, need to be short compared to the rf period.

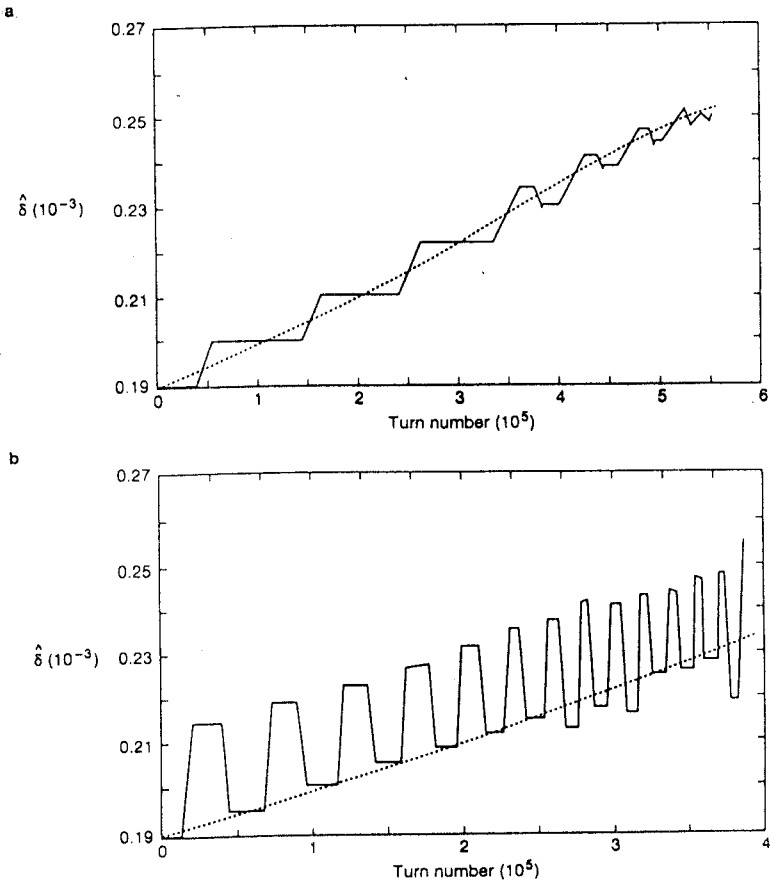

Fig.3. Relative momentum deviation amplitude $\hat{\delta}$ as a fuction of turn number for a halo particle driven by a multiple resonance sequence (solid lines) and by a single resonance sequence (dotted lines). For the pulse duration 13.3 ps (*a*) and 267 ps (*b*)

Because the rf voltage varies sinusoidally in time, the period of a synchrotron oscillation depends on the amplitude of the oscillation. Thus, to increase monotonically the synchrotron amplitude of driven halo particles, the time interval between two successive perturbing pulses has to follow the increase of the synchrotron period. The time sequence of perturbing pulses is determined by the initial location (l_p, δ_p) of the driven halo particles and the

pulse voltage V_p. This sequence when only one perturbing pulse is turned on during a synchrotron oscillation was called a single resonance sequence. Figure 3 shows the growth of the synchrotron amplitude $\hat{\delta}$ of a halo particle driven by a single resonance sequence.

A single resonance sequence determined by the phase space point (l_p, δ_p) captures and ejects only the particles whose initial phase space locations are near that point. To eject significantly more of the particles near the synchrotron orbit passing through (l_p, δ_p) the pulse sequence can be repeated for a number of subsequent turns. This number N_{on} should be less than the number of turns for the halo particle to move along its unperturbed orbit to $(l_p, -\delta_p)$. Otherwise, compensation of the pulse action will occur.

The resulting sequence obtained by repeating the single resonance sequence was called a multiple resonance sequence. Figure 3 shows the growth of momentum deviation amplitude $\hat{\delta}$ due to a multiple resonance sequence. In contrast to the nearly linear growth in the single resonance case, the amplitude growth is not monotonous in the multiple resonance case. However, for pulses both with a small duration (a), and with a large one (b) the average rate of the amplitude growth appears to follow the growth rate in the single resonance case. At that with long perturbing pulses, the multiple resonance sequence is also effective in ejecting the halo particles with $\hat{l} > l_p$ whose initial momentum amplitudes are not near $\hat{\delta}_p$.

So, with the accurate positioning of perturbation pulses in rf phase, one can eject particles only from the tail of the beam without perturbing the core. The ejection efficiency and rate may be regulated by the pulse voltage, the pulse duration, and the resonance repetition number. Moreover, it is possible to act either on a single bunch or on a few bunches simultaneously.

The longitudinal tails of the bunch can be resonantly excited also by the transverse kicker to increase betatron oscillation amplitudes and thus bring particles onto a bent crystal for extraction. Here we review simulation results on a mean impact parameter versus extraction rate for the Tevatron [9]. Kicks were simulated as short electric pulses applied to the tails of a bunch, to guarantee that the core of the bunch will not be disturbed. Applying a kick in a resonant mode with $|\Delta Q| < 0.25$, i.e., approximately each seventh turn, the authors studied an impact parameter distribution at the crystal.

The scheme of the Tevatron is presented in Fig.4. For the simulations,the crystal position was chosen at the E853 [5] crystal position at C0 on the radius of 3 mm outside the beam position. A simple linear model of the Tevatron was used, a matrix transformation of particle parameters — X, X', Y, Y', E, Z — from one location to another. Locations used were present RF position (a kicker was

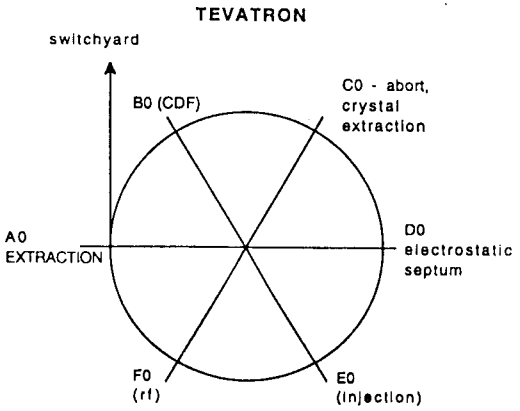

Fig.4. The scheme of the Tevatron

also placed there), B0 and D0 positions, where a head-on beam-beam interactions were simulated, and the crystal position in C0. Initial particle parameters were simulated by Monte Carlo according to the Tevatron emittance parameters. The model was built initially for the SSC collider and was adopted to the Tevatron lattice.

According to the simulation, a mean impact parameter is strongly dependent on the kick value applied. Figure 5 illustrates this. Extrapolation of data to the mean extraction time of 10^6 s, which corresponds to 10% of full beam intensity to be extracted in about 24 hours, predicts a mean impact parameter less than 0.01 μm, too small to make a simple crystal extraction scheme to be practical. Of course, a mean impact parameter value could be dependent on a beam excitation mechanism. However, we are very skeptical to the opinion that some more sophisticated RF gymnastic could be found in colliders which provides a good impact parameter and at the same time satisfies non-interfering requirements. We believe that the good solution of this problem lies in quite different approach [8].

B. Ultrathin Crystal Scatterer — Crystal Mirror. The dominant transverse emittance growth mechanisms predicted for the Tevatron colliding beams are intrabeam scattering and beam-beam interaction. The quality of the linear aperture generally defines long-term beam stability and formation of the beam halo. The head-on beam-beam effect is the major source of nonlinearities. The strongly nonlinear beam-beam force excites high order betatron resonances causing particles to diffuse into the tails of the transverse distributions and to be lost.

For the Tevatron in the colliding mode the measured value of the particle loss on scrapers placed at 10 σ from the design orbit, where σ is the rms transverse size of the beam, is about 0.4×10^7 protons per second for 10^{12} particles in the beam [10]. This corresponds to a beam lifetime of about 70 hours. The projected proton intensity for the Tevatron collider is 5.4×10^{12} [11], which implies proton loss of about 2×10^7 protons per second. It was

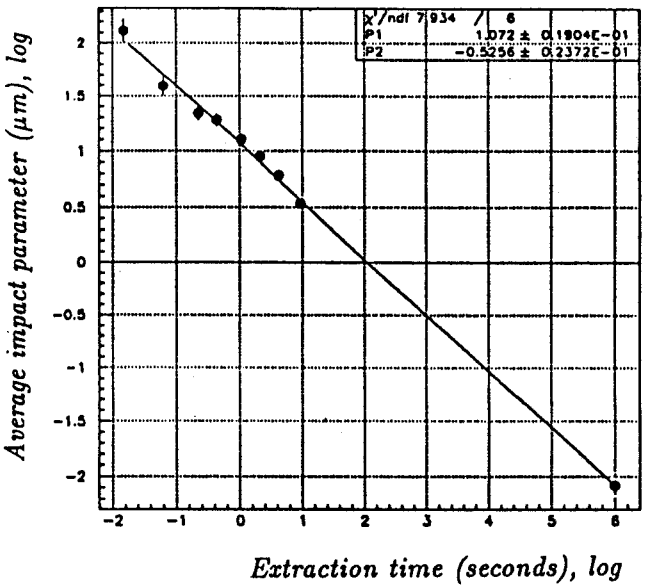

Fig.5. Interpolation of the simulation data for the resonance transverse excitation of the longitudinal halo of the Tevatron beam to the extraction time of 10^6 s. Corresponding mean impact parameter is equal to 0.0083 μm

shown in [8], that practically all these particles could be channeled in a bent crystal and delivered to the extraction line.

As was mentioned already, there is a serious difficulty with delivering the beam into the extraction septum. If we suppose that the halo particle moves away from the beam center at a typical rate of about 0.1 mm per hour, we get a one turn step size of less than the size of an atom [12]. Of course, an accelerator is not such a precise machine. Nonlinear effects due to multipole magnetic components produce turn-to-turn variations of a particle trajectory. Vibrations of quadrupoles, dipole power supply ripple and other noise sources produce a beam position jitter. This could produce an impact parameter at a crystal perhaps of an order of fraction of micrometer. Still, a simple crystal extraction scheme would not be effective under these conditions because of the large ratio of septum thickness to mean impact parameter. Radiation damage to the crystal, which usually does not present a problem [13], in this case could be worsened because of the very high spatial density of radiation, and would reduce the channeling transparency of the crystal.

Placing a crystal at a radial distance of 16-20 σ could partially solve the problem. At this distance particles have stable trajectories for only several turns and are well scattered in space. However, this is not really feasible because scrapers must be placed at about 10 σ to control the beam loss.

One could overcome the difficulty of delivering halo beam particles well into the crystal septum by using a crystalline scatterer. This idea and its application to the SSC were examined in 1991 [14]. Instead of impinging directly on the bent crystal, a particle first hits a thin crystalline scatterer placed at the proper radial distance. To scatter a particle in the horizontal direction, crystalline planes are placed vertically.

The crystal which thickness equals a quarter of oscillation wavelength of particles in the planar channel works as a good scatterer. It broadens the angular distribution of incident beam particles. However, a large part of incident particles gets small angular deflections, smaller than the critical channeling angle. They will form a maximum at the edge of the crystal deflector when such a scatterer is used to throw circulating particles over the imperfect layer at the bent crystal surface.

It was proposed in [8], as a development of an idea of a crystalline scatterer [14], to align a scatterer along the beam with an angular offset of about 1/2 of a critical angle, which makes the scatterer a «crystal mirror». Planar channeling in such a mirror gives particles a kick, in a proper direction, of about a critical angle of channeling, 17 μrad for a tungsten (110) plane. The optimal thickness of the crystal mirror in this case is one-half of a channeling wavelength, because, in the first approximation for the parabola-like plane potential this thickness images a parallel beam into a parallel beam. For the tungsten (110) plane and a proton energy of 900 GeV this thickness is about 24 μm, and about 42 μm in the case of silicon. For a beam with small angular divergence, more than half of the incident particles are reflected in one pass, and this probability rises due to multipass mode.

When a crystal is used as a mirror to throw halo particles of a circulating beam over the crystal surface edge, the maximum of the impact parameter distribution will be far enough from the crystal edge. Therefore, a particle loss on the imperfect layer becomes smaller than with amorphous scatterer or with crystal scatterer of 1/4 wavelength [11]. The remarkable peculiarity of such a scatterer is the small thickness needed to give the particle a large angular deflection, because scattering of particles occurs when the contributions of crystal atoms are added coherently. It is important because the particle loss due to inelastic interactions with scatterer atoms will be considerably smaller in this case. Besides, a crystalline scatterer provides an angular deflection in only one plane, perpendicular to the crystallographic planes.

An amorphous scatterer is less effective than the crystalline scatterer because of the much larger thickness required. To provide the same scattering

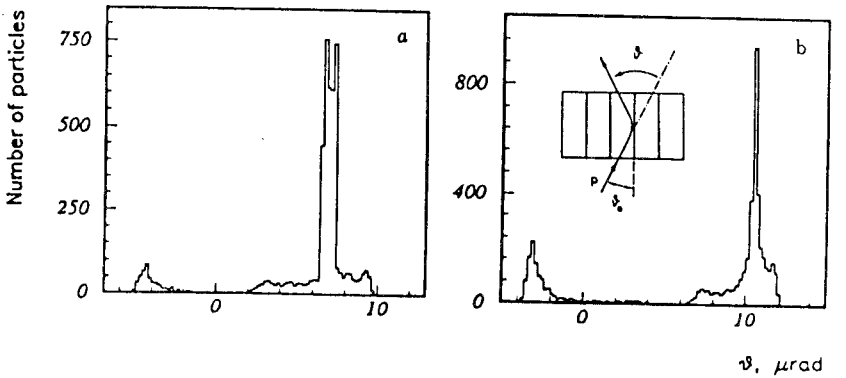

Fig.6. Illustration of using ultrathin crystal as a crystal mirror. Angular distributions of particles outgoing from the silicon crystal for the cases when its (110) planes are tilted by 3.5 μrad (*a*) and 5.25 μrad (*b*) relative to the direction of the incident beam of protons with energy 900 GeV. The insertion in (*b*) shows the trajectory of particle reflected by the crystal plane

angle, 17 μrad, a 0.4 cm thick amorphous tungsten scatterer would be required. The rate of nuclear interactions in such a scatterer would amount to about 7%, which would preclude to use such a scatterer in a multipass mode. Besides, it always gives a maximum of an impact parameter distribution at the edge of the crystal.

Figure 6 demonstrates angular distributions of outcoming particles for different tilt angles of 900 GeV parallel proton beam with the silicon scatterer of 42 μm thickness (a Monte Carlo simulation). The large part of the particles are mirror reflected, their deflection angles are twice more than the tilt angle. Figure 7 presents the mean deflection angle of protons versus the tilt angle of the silicon scatterer. One can see the ability and limitations of the «crystal mirror» technique.

At a typical thickness of 20-40 μm angular miscut, nonflatness, other crystalline defects on the crystalline scatterer do not present serious problems. However, to reduce a problem one can use a very thin amorphous target as a prescatterer. A 20-μm thick amorphous tungsten prescatterer is a proper choice for the Tevatron, providing about 1 μrad angular kicks for particles in both planes due to multiple scattering. At a radial position of 10 σ it gives a mean impact parameter at the crystalline scatterer of about 1 μm. Naturally, the amorphous target has no edge problems similar to the crystalline one. If a particle did not pass through the full thickness of the prescatterer at the first strike, initial angular disturbance due to multiple scattering will be increasing

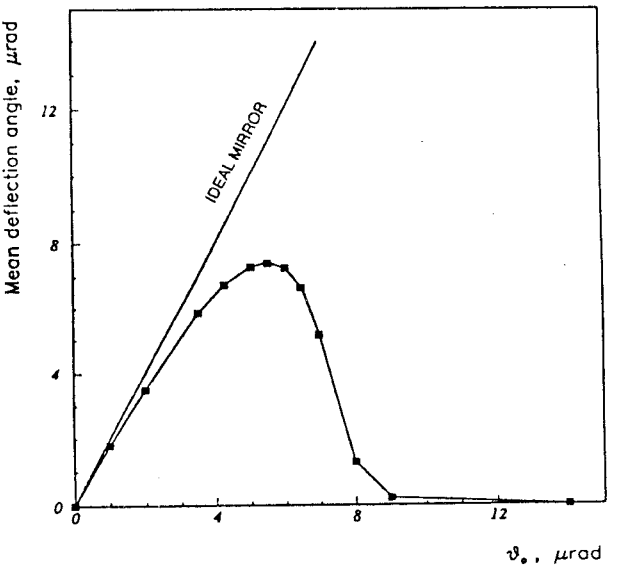

Fig.7. The mean deflection angle of 900 GeV protons by the silicon scatterer *versus* its tilt angle. The straight line corresponds to the case of an ideal mirror

with the subsequent passes until, finally, a particle will go into the bulk of a prescatterer material and undergo a full multiple scattering.

C. Beam Halo Extraction Scheme and Simulation Results. During fixed target runs, the electrostatic septum placed in D0 straight section of the Tevatron provides a 50 μrad kick and drives 900 GeV protons to the extraction Lambertson magnets in A0. Therefore, a 100 μrad bend in a crystal septum would be quite enough to extract beam halo particles. Placed at radial distance of 10 σ, a crystal septum gives a particle an angular kick of about 10 rms beam divergence, therefore providing a necessary separation of its trajectory from the main circulating proton beam.

The authors [8] made quite detailed Monte Carlo simulation of the Tevatron beam halo extraction. The location of the bent crystal was chosen again at the C0 straight section at the azimuth of E-853 experiment [5]. Here we remark that although all calculations have been made for the C0 section, results on the bending efficiency are generally applicable to the most of the azimuthal positions in the Tevatron.

The scheme of the extraction is presented in Fig.8. The extraction system could be placed either in the horizontal or in the vertical plane. The extraction

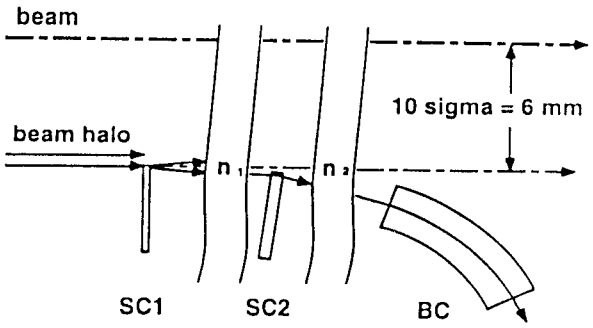

Fig.8. The diagram of crystal extraction. SC1 — amorphous prescatterer, SC2 — crystalline scatterer, BC — bent crystal, n — number of turns necessary for a particle to hit the next target. SC1: Scatter foil 20 μm W; SC2: Crystal foil 42 μm Si; BC: Bent Crystal 5 mm Si. n1: number of turns to hit crystal foil, typically about 300. n2: number of turns to hit bent crystal, typically 7–20. SC1, SC2, BC are mounted on an optical table and aligned with tolerances about 1 μm

device consists of an amorphous prescatterer, SC1, a crystal scatterer, SC2, and a bent crystal septum, BC. Although the most efficient azimuthal positions for all three extraction elements would be different for each element, the same azimuthal position for all of them was used in studies to simplify the calculations and present a more practical case. In the simulation, the crystal scatterer was placed immediately behind the bent crystal in the beam direction, and the amorphous prescatterer was placed immediately behind it. The radial position of the SC1 was chosen to be 6 mm, i.e., 10 σ. Typically, a 20 μm thick amorphous tungsten prescatterer SC1 was used with an rms multiple scattering angle of 1 μrad. The inner edges of the crystal scatterer SC2 and the bent crystal BC would be additionally shifted from the beam orbit. The radial positions of SC2 and BC were varied to obtain an optimum for the extraction. The results are typically obtained for the case with the bent crystal radial offset of 15 μm relative to the SC2, that is close to optimal with respect to the loss in an imperfect surface layer. The authors used a geometry in which particles were deflected in the horizontal plane.

Beam dynamics in the accelerator enhances performance of the bent crystal as an extraction device. Due to very slow transverse diffusion, beam halo particles that encounter the crystal extraction system have a very narrow angular spread (quasi-parallel beam), therefore providing a very high channeling efficiency. In addition, due to the small scattering angles involved, a scattered particle will make multiple passes through the bent crystal, increasing the probability of channeling. These two circumstances drive up the extraction efficiency significantly.

The particle orbits were calculated for the two-dimensional (X-S) case. If the halo formation is going independent in the X- and in the Y-plane, only half a halo will be extracted by one crystal and another half will be scraped by the

Y scraper. In this case one should place a similar extraction system in the Y-plane to extract all the halo particles. The authors believe, however, that the halo particles of large amplitude oscillations in the *X*-plane have large amplitudes also in the *Y*-plane, and *vice versa*. In this case a bent crystal extraction in one plane will work as an efficient drain for all the halo particles.

Particle trajectories both in the crystal scatterer SC2 and in the bent crystal BC were calculated by a numerical solution of the equations of motion in the potential of bent atomic planes. After a step size, which is much smaller than the wavelength of a particle oscillation in the channel, the change of transverse velocity due to multiple scattering was computed. More details of these simulations can be found in reference [15]. The model describes well all the existing experimental results on channeling with bent crystals.

A full simulation code was used that combines collider simulation with tracking particles in a crystal. The code is based on previous studies [16] and was adopted for the Tevatron lattice.

To simulate the beam halo, initial values X, X' of particles were generated at the bent crystal position using a uniform phase distribution and a flat distribution from 6 mm to 6.0001 mm for the particle amplitudes X_m. Typically, 1000 particles were generated for each version of initial conditions. After the first collision with the amorphous prescatterer SC1, which gave a particle an angular rms kick of 1 μrad, a particle traveled typically many turns before it hits the crystal scatterer SC2, placed at a radial position of 6.001 mm, i.e., outward from SC1 by 1 μm. A full turn transfer matrix for the *X*-plane was used to transport particles through the accelerator ring.

As was mentioned before, the authors use a crystal SC2 as a crystalline mirror with a tilt angle of about 1/2 of the critical channeling angle. Figure 9 shows typical impact parameter distributions at the bent crystal position for the cases when the silicon (a) and tungsten (b) scatterers were used. The scatterer SC2 clearly works as a crystal mirror. The distribution maxima are far enough from the crystal edge. So, the thin tungsten crystalline mirror increases the mean impact parameter at the bent crystal to about 200 μm.

Most of the particles that hit the bent crystal BC can be captured into channeling regime by the bent planar channels. These particles are deflected at a bending angle if they are not dechanneled due to multiple scattering by crystal electrons and nuclei, and do not experience nuclear interactions. Another part of particles will experience multiple scattering in the crystal (that is rather small) or could be lost due to inelastic nuclear interactions. After multiple scattering in the bent crystal, particles continue to travel around the accelerator and strike the bent crystal again. The authors [8] assume that a particle is extracted if it leaves from the crystal at the crystal bending angle, within the critical angle of channeling. It was also assumed that the imperfect layer 0.5 μm thick exists at

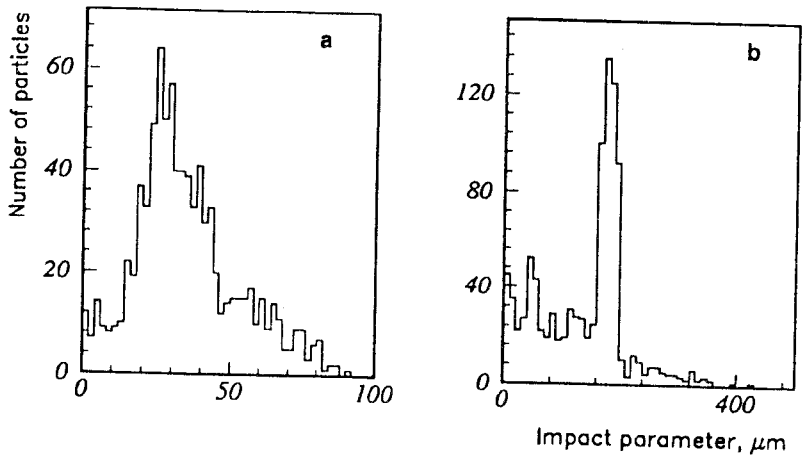

Fig.9. The impact parameter distributions of protons at the bent crystal when different crystal mirrors SC2 were used: *a* — silicon, *b* — tungsten

the crystal surface. These imperfections can include short planar channels due to a crystal miscut or surface planar channels with shorter dechanneling length than in the body of the crystal. These give particles large angular deflections, but do not allow them to be extracted. It is probably a stricter limitation than in reality.

The calculations were continued until all the particles end the process being extracted, or experience a nuclear interaction, or being lost in the imperfect surface layer, or dechanneled and lost in the accelerator.

Cooling the bent crystal allows one to reduce dechanneling and therefore the particle losses in the crystal. The results of simulation presented below for the bending angle of 100 μrad and a 5 mm long silicon crystal were obtained for the case when the crystal was cooled to 4K. For the optimum orientation angle of the bent crystal, which is about 4.5 μrad, the extraction efficiency was 0.988. For comparison, in the case without crystal scatterer, i.e., when the tungsten amorphous prescatterer was used only, the extraction efficiency was equal to about 60%. It is much smaller yet for the case of a bent crystal alone due to larger particle losses in the imperfect crystal layer.

The fraction of protons extracted at the first passage through BC decreases fast with the crystal disorientation, Fig.10*a*. However, a total extraction efficiency decreases less than 10% in the angular range of 10 μrad due to the contribution of multiple passages of particles through the crystal deflector. Figure 10*b* presents the extraction efficiency versus SC2 orientation. Again, there is no sharp efficiency dependence on SC2 orientation, due to multiple passages

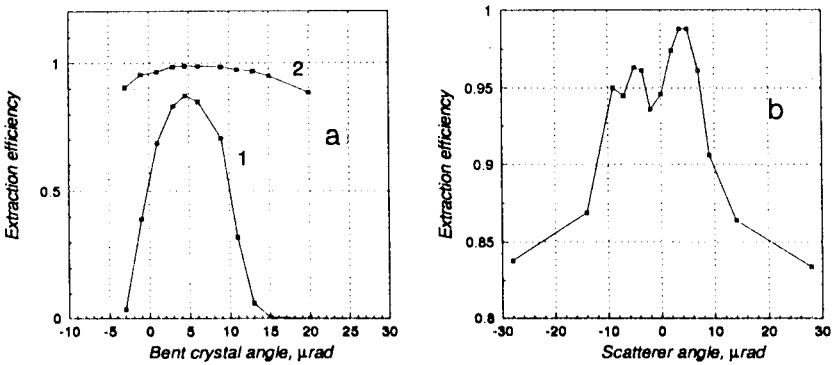

Fig.10. Extraction efficiency *versus* bent crystal orientation (*a*), curve 1 — first hit extraction, curve 2 — multipass extraction, and *versus* crystal scatterer orientation (*b*)

through the crystal deflector BC. However, if one needs to reduce particle loss during extraction to the level of less than 10%, a careful orientation of SC2 should be done because width of local maxima is of about a channeling critical angle. The left local maximum in Fig.10*b* is suppressed in comparison with the right one because BC orientation for these calculation was optimized for the right one.

The radial offset of the bent crystal BC relative to the crystal scatterer SC2 could be also important to get the highest extraction efficiency. There is no strong efficiency dependence when this offset is bigger than 5 μm. For small offset of about 1 μm there is a large fraction of particles which are not mirror reflected in SC2. They hit the bent crystal near its inner edge. This leads to the efficiency decrease because of the particle loss in the imperfect layer.

A 100 μrad bend was considered as the most efficient. Extraction efficiency was studied also for a 600 μrad bend and for a 3 mrad bend, and happen to be 0.981 and 0.840, correspondingly.

II. BEAM IMPROVEMENTS AND BEAM DIAGNOSTICS

A. Collider Model. Few years ago a Monte Carlo computer code was developed [17] to simulate the decoherence of beam oscillations in the SSC collider due to the tune spread generated by the head-on beam-beam interaction. The code was proven to be a reliable tool in studies of major beam dynamics in colliders and recently was successfully applied to the LHC. The results of the simulations [17] were compared with previous theoretical estimates on the decoherence time [18], and sufficient disagreement was found.

In a collider, there exist many external circumstances in which the centroid of a circulating beam is displaced from the design orbit. If particle motions are linear, the displaced beam will undergo betatron oscillations as a whole (coherently) because all particles in the beam have the same tune, defined by the number of betatron oscillations in one revolution. However, nonlinearities in the machine can cause different particles to have different tunes, i.e., can generate a tune spread in the beam. When this is the case, the betatron motions of particles in a displaced beam will not be coherent, and the so-called phase mixing or decoherence results. Eventually, the phase space distribution of the beam will approach an equilibrium with the beam centroid returning to the design orbit, and the beam size (emittance) enlarged. For the SSC Project, the tune spread was primarily generated by the nonlinear Coulomb force experienced by the two counter-rotating beams when they collide at the interaction points, i.e., the so-called head-on beam-beam interaction.

In the paper [17], using the so-called weak-strong model, the authors simulated the head-on beam-beam interaction for the SSC Project in the two low-β IRs and estimated the decoherence time of an initially displaced beam in the presence of the beam-beam interaction.

Particles were tracked in the four-dimensional phase space (X, X', Y, Y') using a linear lattice for the SSC collider. Three locations in the lattice have been considered: the two interaction points IP1 and IP2, and the location M where the beam positions are measured. The Table lists the relevant lattice parameters at these three locations.

The initial values of X, X', Y, Y' of the particles were generated at the location M using Gaussian distributions with a normalized emittance of $\varepsilon_N = 1$ mm·mrad for both X and Y directions. The initial rms beam size in one

Table. SSC Project lattice parameters at locations IP1, IP2 and M

	IP1	IP2	M
S	36 947.925 m	39 467.925 m	86 525.550 m
α_x	− 0.003	− 0.015	0.115
β_x	0.501 m	0.502 m	427.477 m
α_y	− 0.024	0.001	− 0.495
β_y	0.505 m	0.493 m	533.929 m
Q_x	52.022	56.275	122.735
Q_y	51.138	55.385	121.753

S: path length; α, β: usual Courant-Snyder parameters; Q_x, Q_y: tune advances. The total tune advances in one revolution are: $\nu_x = 123.285$ and $\nu_y = 122.265$.

direction is then $\sigma = 140$ μm. Once generated, the initial beam was displaced horizontally by an amount ΔX_0, i.e., for every particle $X_i \to X_i + \Delta X_0$. Three transfer matrices were then used to carry the particles once around the collider ring: from the location M through the interaction points IP1 and IP2, and back to the location M. Typically 10,000 particles were tracked for 5,000 turns. At the interaction points, particles were given kicks due to the Coulomb force between the particle and counter-rotating bunch, so that their angles were changed to

$$X' \to X' + \Delta X', \quad Y' \to Y' + \Delta Y'. \tag{1}$$

The kicks, $\Delta X'$ and $\Delta Y'$, were calculated using the weak-strong model in which the beam under consideration is regarded «weak» and the counter-rotating beam, unperturbed by the weak beam, is regarded «strong». Assuming that the particle distribution in the strong beam is a round Gaussian, i.e., the beam sizes in X and Y directions are the same, the kicks are given by [19]

$$\begin{bmatrix} \Delta X' \\ \Delta Y' \end{bmatrix} = \frac{2N_b r_p}{\gamma_p} \frac{1}{X^2 + Y^2} \left(1 - \exp\left(-\frac{X^2 + Y^2}{2\sigma^2} \right) \right) \begin{bmatrix} X \\ Y \end{bmatrix}, \tag{2}$$

where N_b is the number of particles in a bunch of the strong beam, r_p the classical proton radius, γ_p the Lorentz relativistic factor for a 20 TeV proton, and σ the rms beam size at the low-β IPs. The authors have used $N_b = 0.8 \times 10^{10}$ and $\sigma = 5$ μm in accordance with the SSC baseline design. In the formula (2) X and Y are the real positions of particles in the weak beam with respect to the design orbit, which is fixed and coincides with the beam centroid of the strong beam.

After each turn, at the location M, the authors calculated the beam centroid in phase space

$$X_c = \frac{1}{N} \sum_{i=1}^{N} X_i, \quad X'_c = \frac{1}{N} \sum_{i=1}^{N} X'_i, \tag{3}$$

and the beam emittance relative to the beam centroid

$$\hat{\varepsilon} = \frac{\pi}{N} \sum_{i=1}^{N} (\gamma \hat{X}_i^2 + 2\alpha \hat{X}_i \hat{X}'_i + \beta \hat{X}'^2_i), \tag{4}$$

where $\hat{X}_i = X_i - X_c$, $\hat{X}'_i = X'_i - X'_c$, $\gamma = (1 + \alpha^2)/\beta$, and N is the number of particles being tracked. As we will see below, this relative-to-centroid beam emittance will grow and reach a maximal value in the decoherence process.

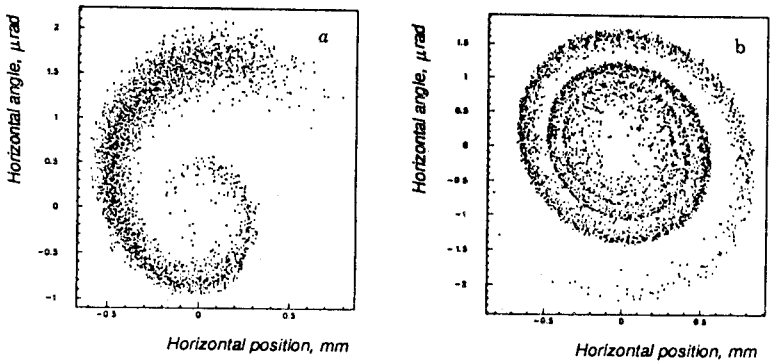

Fig.11. Distributions of the beam in phase space after 1000 turns (*a*) and 5000 turns (*b*). Initial horizontal displacement of the beam $\Delta X_0 = 500$ μm

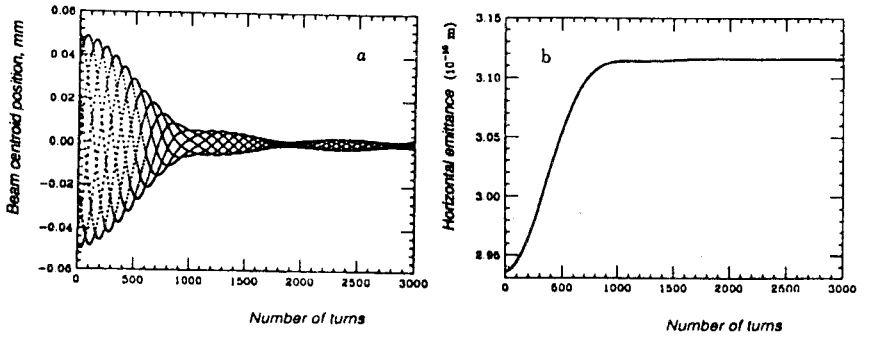

Fig.12. Oscillations of the beam centroid X_c (*a*) and growth of the relative-to-centroid beam emittance $\hat{\varepsilon}$ (*b*) due to the decoherence process after an initial beam displacement of 50 μm

Hence its growth profile is used in the following to characterize the time scale of the decoherence process.

To illustrate the decoherent process due to the beam-beam interaction, we show in Fig.11 the phase space distributions of the beam at 1000 and 5000 turns after its initial displacement of $\Delta X_0 = 500$ μm. Here we see that the beam distribution in phase space is being homogenized. The authors [17] show the time evolution of the centroid position X_c and the beam emittance $\hat{\varepsilon}$ in Fig.12*a,b* respectively for an initial beam displacement of $\Delta X_0 = 50$ μm. Here we see that, as the beam decoheres, X_c oscillates with decreasing amplitude and eventually

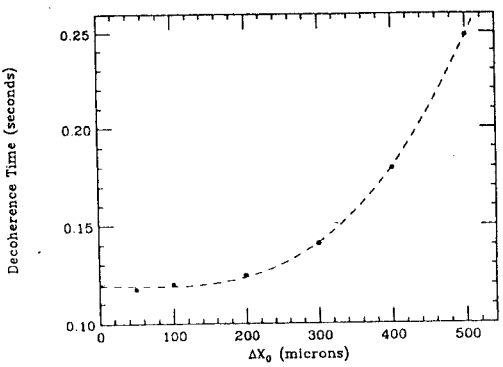

Fig.13. Decoherence times as a function of the initial beam displacement. Circles are the values obtained from the emittance growth profiles using the definition described in the text. The dashed curve is a polynomial fit to guide the eyes

settles around zero (the design orbit), and that $\hat{\varepsilon}$ increases monotonously (on the time scale of a few turns) and finally approaches a steady-state value. Both figures clearly indicate that a new equilibrium is being reached in the beam after an initial displacement. Shown in the figures is typical what will occur during the decoherence process, regardless of the amount of the initial displacement. As discussed earlier, phase mixing of particles due to the tune spread generated by the beam-beam interaction has lead to a new equilibrium in the beam.

It is convenient to use the evolution profile of $\hat{\varepsilon}$ to determine the time scale of the decoherence process or the decoherence time. The authors define the decoherence time to be the time or the turn number at which $\hat{\varepsilon}$ reaches the midpoint between the initial and final values. The decoherence time so defined and its dependence on the initial beam displacement is shown in Fig.13. It appears that the decoherence time remains fairly constant (about 400 turns or 0.12 seconds) for small beam displacements and increases rapidly when the beam displacement exceeds 1.5 σ.

It was reported in [18] that the decoherence time is approximately 0.8 seconds for the SSC. This seems in serious disagreement with our simulation results [17], where it was about 0.12 seconds. Because the decoherence time is an important parameter in the design of feedback systems, it should be estimated carefully. After we pointed out the discrepancy, a more detailed theoretical calculation [20] showed good agreement with our simulation.

B. Compensation of the Beam-Beam Effect in Proton-Proton Colliders. As it was already mentioned, the head-on beam-beam effect is the major source of nonlinearities in high energy colliders. Such a nonlinearity imposes strict limits on the collider luminosity due to the beam instability. The head-on beam-beam instability remains as the most fundamental luminosity limitation for proton-proton colliders. The strongly nonlinear beam-beam force excites high order betatron resonances, so particles diffuse into the tails of the transverse distributions and get lost. For the SSC collider Project the beam-beam

interaction luminosity limit was about 3×10^{34} $cm^{-2}s^{-1}$, i.e., well above the design luminosity of 10^{33} $cm^{-2}s^{-1}$. However, the tune spread generated by head-on beam-beam interactions causes fast decoherence of the betatron oscillations [17] and, therefore, imposes more stringent requirements on any feedback system. This was especially important for such a low emittance machine as was in the SSC Project. For the LHC collider the beam-beam interaction luminosity limit is about 2.5×10^{34} $cm^{-2}s^{-1}$, i.e., still above the design luminosity of 1.0×10^{34} $cm^{-2}s^{-1}$, but this gap is already not as big as was for the SSC Project. Therefore, for the LHC collider a solution for reducing the head-on beam-beam effect is important.

The head-on beam-beam effect in proton-proton machines might be compensated, under certain conditions, by collisions of the bunch on each turn with a space charge of the opposite sign, for example, with a low energy electron beam. Originally, the idea of a beam-beam effect compensation was suggested in [21].

An ideal solution for compensation of the beam-beam effect in proton-proton machines is an instantaneous collision of a proton bunch with a counter-rotating beam of negatively charged particles having the same parameters as a counter-rotating proton bunch. In this case the angular kick delivered to each primary proton by the space charge of the counter-rotating proton bunch would be exactly canceled by the kick delivered by the space charge of the compensating beam. A low energy electron beam could be proposed as a compensating beam. It is important that the compensating beam be formed with the same two-dimensional transverse coordinate distribution as the proton bunch. The longitudinal profile of the compensating beam is not very important, because the angular kick delivered to the primary proton by the compensating beam could be accumulated along the length of the available collision region (about two meters for the SSC Project and the LHC), which is still short in comparison with a betatron wave length.

Instead of a compensating collision point placed immediately after the proton-proton collision, one can place the collision point in a more accessible location with a betatron phase advance relative to the proton-proton collision point of $n\pi$, where n is integer, the same in the X-plane and in the Y-plane. Here the image of the proton beam in the X—Y plane is similar to the image in the proton-proton interaction point, being different only in scale. By using a place in the lattice with high beta values one could relax the requirement to form a beam of a very small size, as in the low-β IPs.

The current in the relativistic electron beam that is necessary for compensation of the beam-beam effect of the counter-rotating beam is defined by the current of the proton beam and its size. Electron guns with necessary parameters are available from the industry.

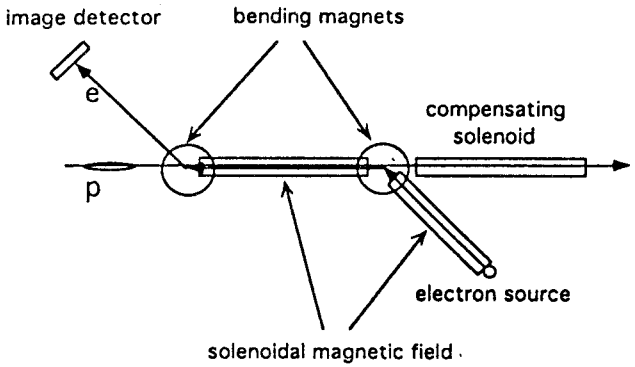

Fig.14. The scheme of a beam-beam compensating device. A low energy electron source collides with a bunch of protons. Electrons are kept stable in space by a solenoidal magnetic field. After collision with the proton bunch an electron beam is deflected to the image detector which is used for steering the electron beam relative to the proton bunch

One of the problems with using a low energy electron beam for beam-beam effect compensation is electron oscillations during passage through the proton bunch. Even passing once and then being dumped, electrons experience some oscillations inside the proton bunch, which makes distribution of proper kicks among all the protons in the bunch difficult. Several different methods were considered by the authors [21] to avoid this difficulty. The ZBEAM tracing code [22] was used to study the electron trajectories inside the proton bunch. It was found that the use of a solenoidal field presents the best solution to the problem. Therefore, for a round Gaussian beam a collision of a proton bunch with a low energy electron beam kept stable by a solenoidal magnetic field will adequately approximate a proton-proton collision with the opposite sign of the effect.

Figure 14 presents a design for a possible device for beam-beam effect compensation. A low energy electron beam, being kept transversally stable by the solenoidal magnetic field, is directed by the deflecting magnets to the interaction region to produce a head-on collision with the proton bunch. The influence of the solenoidal magnetic field on the proton bunch is then compensated by the same field configuration with the opposite polarity.

In paper [23], the authors presented simulation results related to the problem of beam-beam effect compensation for the LHC. The results are summarized in Figs.15,16, where the decoherence time and the rms beam tune spread are plotted versus the electron beam displacement, its relative charge,

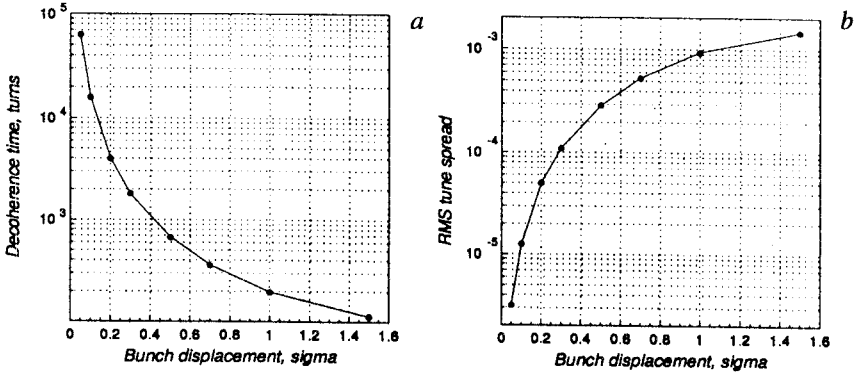

Fig.15. Results of using the beam-beam compensating device. Decoherence time expressed in number of turns (*a*) and rms tune spread of the beam particles (*b*) *versus* displacement of the compensating electron beam from the closed orbit

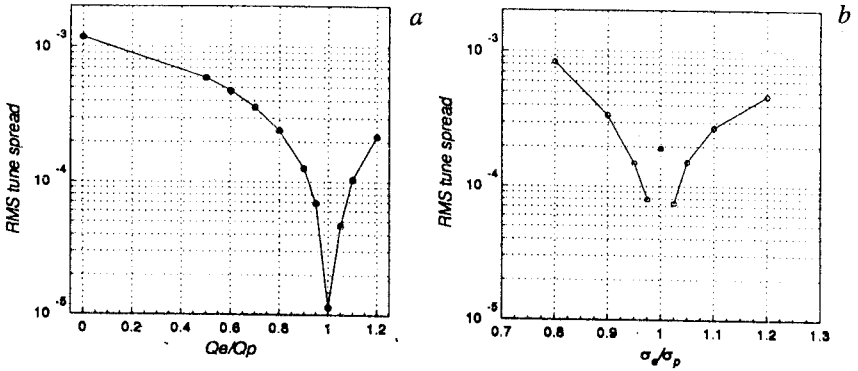

Fig.16. Results of using the beam-beam compensating device. RMS tune spread of the beam particles *versus* the ratio of the electron to proton bunch charges (*a*) and *versus* the ratio of the electron to proton bunch sizes (*b*) (white circles). Displacement of the electron bunch is 0.1 σ. The leftmost point corresponds to the case without compensation

and transverse size. The authors [23] proposed to use a solenoidal magnetic field as a method to prevent electron oscillations. It was shown that in the case of $B = 2$ Tesla for the LHC beam the radial position of a 10 keV electron remains constant with an accuracy of about two micrometers.

The presented results show that in the case of the LHC it is possible to achieve a good beam-beam effect compensation with the resulting reduction of

the beam tune spread by a factor of up to about 100, with reasonable tolerances on the electron beam parameters. Further increase of the design LHC luminosity becomes in principal feasible.

C. Intelligent Damper System. A novel transverse beam damper system improving stability against ground motion, resistive wall instabilities, and other effects in colliders was proposed and developed during the SSC Project evaluation [24]. The novel feature of the system is the use of two kickers, which permits almost exact orbit compensation within one turn.

Transverse damping is very important for large circular accelerators, such as the LHC, because of resistive wall instabilities, motion of quadrupoles due to ground motion, power supply ripple in dipoles, etc. A minimal transverse damping system consists of one Beam Position Monitor (BPM), followed downstream, with betatron phase advance that is an odd multiple of $\pi/2$, by one kicker. For a beam bunch oscillating with optimal phase, this configuration can provide single turn, unity-gain damping. That is, the kicker can cancel the full betatron oscillation measured by the detector the first time the bunch passes the kicker.

This minimal scheme has two disadvantages. One is the operational difficulty of preserving the required betatron phase relationship between pick-up and kicker as the lattice optics are altered. This is especially true because according to transit time requirements the kicker to be displaced by a large fraction of the ring circumference. A well-known fix for this problem is to provide two pick-ups, separated by roughly $\pi/2$ in phase.

The other problem with the minimal scheme is that the phase of the bunch is uncertain, and instead of full cancellation, damping of the betatron oscillation is provided only in some number of turns that depends on the lattice tune. Proposed scheme [24], requiring the use of two kickers, spaced presumably by $\pi/2$, is able to cancel the oscillations for each bunch exactly, not just statistically. This cancellation is independent of the betatron oscillation phase. Damping of the transverse bunch oscillations may be treated as a pure trajectory task and, in a linear machine approximation, has an exact, single turn, solution, not just a statistical solution. Of course, the precision with which this can be accomplished depends on the accuracy of the beam position monitors.

Damping systems with two BPMs and two kickers have been discussed before [25,26,27,28], but without elimination of phase dependence. The proposed scheme provides improved damping of instabilities with shorter growth times and noise sources of greater amplitude.

A simplified diagram of the proposed two-BPM, two-kicker scheme is shown in Fig.17. As far as we know, the basic idea is original. It can be called «intelligent» in that it is assumed that a certain amount of calculation can be performed in the time available before the kicker voltage is applied.

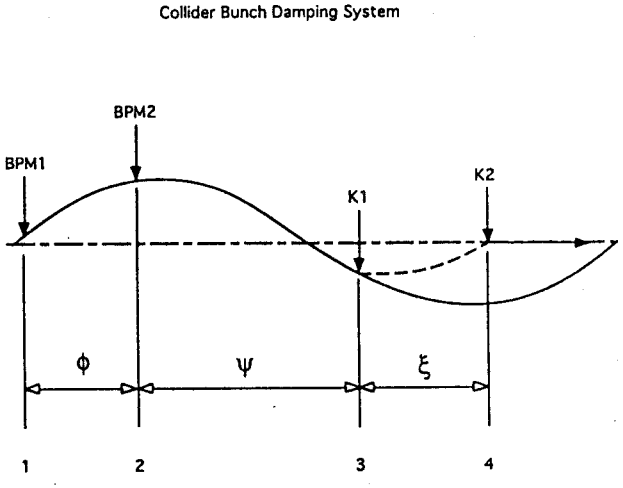

Fig.17. Collider bunch-by-bunch transverse damping system. Kickers K1 and K2 apply kicks calculated from displacements X1 and X2, measured at BPM1 and BPM2. Betatron phase advances between elements ϕ, ψ and ξ, are defined as shown. The solid line is the uncorrected trajectory. The dashed line is the corrected trajectory

Let us consider fully decoupled motion restricted to a single plane, say horizontal. Two beam position monitors, BPM1 and BPM2, separated by betatron phase angle ϕ, measure horizontal positions of the bunch in two locations along its orbit. This information is processed, and correction signals are sent to two kickers, K1 and K2, separated by approximately $\pi/2$. To simplify the picture, it will be assumed that the gain of the electronics is 1. At the first kicker K1 an angular kick is produced which sets the slope of the bunch motion X' to some value, X'_3, which is necessary to bring a bunch at the K2 position with zero displacement. Let us bring the bunch from point 3 to point 4

$$\begin{pmatrix} X_4 \\ X'_4 \end{pmatrix} = \begin{pmatrix} \left(\frac{\beta_4}{\beta_3}\right)^{1/2} (\cos\xi + \alpha_3 \sin\xi) & (\beta_3\beta_4)^{1/2} \sin\xi \\ \frac{1+\alpha_3\alpha_4}{(\beta_3\beta_4)^{1/2}} \sin\xi + \frac{\alpha_3-\alpha_4}{(\beta_3\beta_4)^{1/2}} \cos\xi & \left(\frac{\beta_3}{\beta_4}\right)^{1/2} (\cos\xi - \alpha_4 \sin\xi) \end{pmatrix} \begin{pmatrix} X_3 \\ X'_3(a) \end{pmatrix},$$

where $X'_3(a)$ is the slope of a bunch after the K1. Here α_i and β_i are the Courant-Snyder parameters of the lattice.

Therefore,

$$X_4 = (\frac{\beta_4}{\beta_3})^{1/2} (\cos \xi + \alpha_3 \sin \xi) X_3 + (\beta_3 \beta_4)^{1/2} \sin \xi \, X'_3(a).$$

Because we are seeking $X_4 = 0$, then

$$X'_3(a) = -\frac{1}{\beta_3} (\cot \xi + \alpha_3) X_3,$$

where

$$X_3 = (\frac{\beta_3}{\beta_2})^{1/2} (\cos \psi + \alpha_2 \sin \psi) X_2 + (\beta_3 \beta_2)^{1/2} \sin \psi \, X'_2,$$

where

$$X'_2 = \left[-\frac{1 + \alpha_1 \alpha_2}{(\beta_1 \beta_2)^{1/2}} \sin \phi + \frac{\alpha_1 - \alpha_2}{(\beta_1 \beta_2)^{1/2}} \cos \phi \right] X_1 + \\ + (\frac{\beta_1}{\beta_2})^{1/2} (\cos \phi - \alpha_2 \sin \phi) X'_1,$$

where

$$X'_1 = \frac{X_2}{\sin \phi \, (\beta_1 \beta_2)^{1/2}} - \frac{X_1}{\beta_1} (\alpha_1 + \cot \phi).$$

At the same time, the slope of the bunch before K1 $X'_3(b)$ is

$$X'_3(b) = \left[-\frac{1 + \alpha_2 \alpha_3}{(\beta_2 \beta_3)^{1/2}} \sin \psi + \frac{\alpha_2 - \alpha_3}{(\beta_2 \beta_3)^{1/2}} \cos \psi \right] X_2 + \\ + (\frac{\beta_2}{\beta_3})^{1/2} (\cos \psi - \alpha_3 \sin \psi) X'_2.$$

Therefore, the necessary kick $\Delta X'_3$ is

$$\Delta X'_3 = X'_3(a) - X'_3(b). \tag{5}$$

Again, from the matrix transformation,

$$X'_4 = \left[-\frac{1 + \alpha_3 \alpha_4}{(\beta_3 \beta_4)^{1/2}} \sin \xi + \frac{\alpha_3 - \alpha_4}{(\beta_3 \beta_4)^{1/2}} \cos \xi \right] X_3 + \\ + (\frac{\beta_3}{\beta_4})^{1/2} (\cos \xi - \alpha_4 \sin \xi) X'_3(a).$$

To bring the bunch slope to zero after K2, the necessary kick is

$$\Delta X'_4 = - X'_4. \tag{6}$$

Eq.(6) can be simplified immediately if the optional choice, $\xi = \pi/2$, has been made. However, it is not essential for that condition to be satisfied exactly.

The computations needed to determine kicks $\Delta X'_3$ and $\Delta X'_4$ can be expressed as two linear relations

$$\Delta X'_3 = a_1 X_1 + a_2 X_2, \tag{7}$$

$$\Delta X'_4 = b_1 X_1 + b_2 X_2, \tag{8}$$

where constants a_1, a_2, b_1, and b_2, are precalculated from the lattice constants. Since the phase differences ϕ, ψ and ξ are functions of the tune these constants must be recalculated when the lattice is retuned.

To insure that the information from BPM1 and BPM2 is maximally independent, which optimizes the accuracy of $\Delta X'_3$ and $\Delta X'_4$, their phase separation should approximately satisfy the condition $\phi \simeq \pi/2$.

In any practical system, since the bunch will outrun any correction signal to downstream kickers, one must wait for almost one revolution of the bunch around the collider circumference. This sets a natural limit on the performance of the damping system. All stochastic deviations accumulating in one turn can then be corrected after an additional turn.

The configuration can be used for bunch-by-bunch damping. If digital arithmetic is used, analog-to-digital conversion of bunch displacements, for colliders similar to the SSC, must occur at the 60 MHz bunch passage frequency, and performing the calculations of Eqs.(7) and (8) must proceed at a 240 Megaflop rate. Also the kicker rise time must correspond to the same 60 MHz frequency. It appears at present time to be technically possible to meet these requirements.

The damping system proposed could be used for all stages of collider ring operation — injection, acceleration, collision — if the dynamic range of the apparatus is made wide enough, from micrometers to millimeters.

D. Electron Beam Probe for Beam Diagnostics. Recently, a low-energy electron beam was proposed [29] for nonperturbing diagnostics of high-energy electron beams, based on earlier works [30]. This approach could be applied to any high energy collider for precise and nondisturbing beam diagnostics.

A diagram of the beam emittance monitor for high energy colliders using a low-energy probe electron beam is presented in Fig.18. An electron gun directs a 10-keV electron beam perpendicular to a proton beam. Deflected electrons are detected with a position sensitive detector. The monitor can use a well-focused electron beam sweeping through the proton beam, or a wide, parallel electron

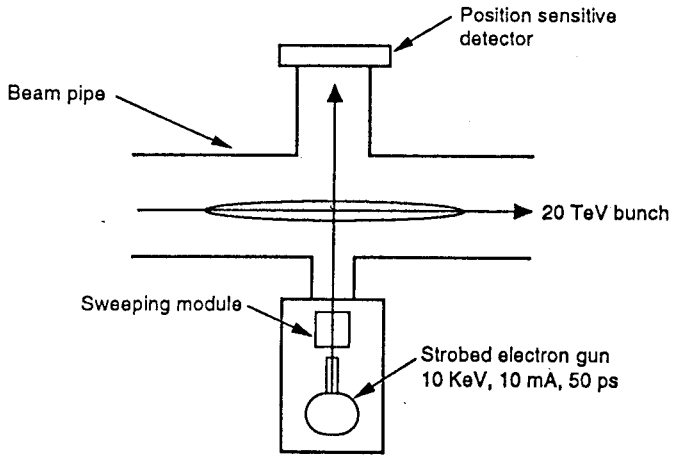

Fig.18. Electron beam profile monitor for a high energy collider

beam. Single bunch measurements are possible in the latter case, i.e., when illuminating a bunch of high-energy particles by a wide parallel electron beam one can obtain a specific «shadow picture» of the proton bunch.

The authors [29] used the ZBEAM simulation code [22] to trace probe electrons in the vicinity of a 20 TeV beam of the SSC Project. The bunch structure of the 20 TeV beam was taken into account. The bunch was considered as a moving charge equivalent to the charge of 10^{10} protons with three-dimensional Gaussian distribution in space. A Gaussian distribution with $\sigma_z = 5$ cm was used in the Z-direction. For a round Gaussian, $\sigma_x = \sigma_y$, different transverse beam sizes were considered. The electrons were exactly synchronized with the proton bunch. The Z-component of the electrical field of the bunch is rather small, and authors neglect it.

It was found that the electron deflection angle is quite sensitive to the position of the electron beam inside the proton bunch. Figure 19*a* presents the deflection angle of the electron versus its distance from the center of the proton beam (impact parameter) for different beam sizes. By measuring the deflection of the electron beam, it is possible to obtain the rms transverse size of the beam with good precision. The probing electron beam would be swept across the main beam to obtain a full deflection profile. Electrons should be focused in the plane of the proton beam in a spot less than 10 μm in size in order to not introduce any significant broadening to the measured beam size.

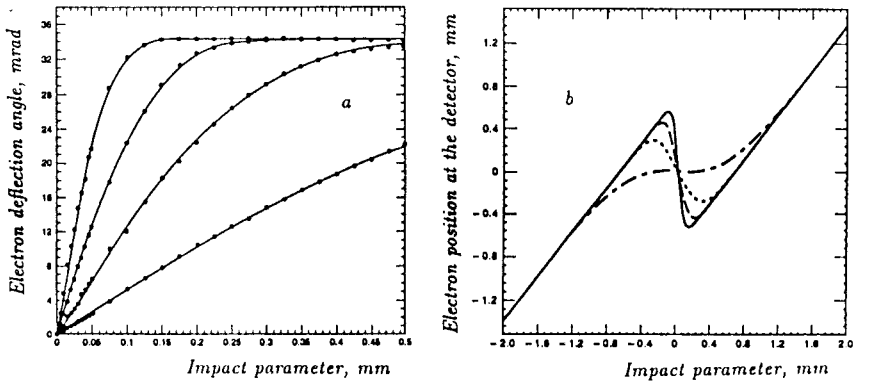

Fig.19. Deflection angle of 10 keV electrons (*a*) and its *X*-position at the detector (*b*) *versus* impact parameter with the proton bunch. The distribution of the proton bunch charge is three-dimensional Gaussian with $\sigma_x = \sigma_y$, μm: 50 (solid line), 100 (dashed), 200 (dotted), 500 (dash-dotted). σ_z = 5 cm

A notable feature of Fig.19*a* is the leveling off of the deflection angle for values of the impact parameter which exceed the *X*-extent of the beam. If the impact parameter *b* is beyond the *X*-extent of the beam, but still very small compared to the *Z*-extent of the bunch, it is reasonable to model the force felt by the probe electron as that due to an infinite line charge,

$$\mathbf{F}(\mathbf{R}) = \frac{-2eq_L\mathbf{R}}{|\mathbf{R}|^2}, \tag{9}$$

where e is the electron's charge, q_L is the linear charge density of the idealized line charge, and $\mathbf{R}$ is the two-dimensional vector (X, Y).

The change in momentum experienced by the electron is given by the impulse produced by this force along the electron's trajectory,

$$\Delta\mathbf{p} = \int_{-\infty}^{\infty} dt\, \mathbf{F}(\mathbf{R}(t)). \tag{10}$$

In our case the electron deflection angles are small enough, $\theta << 1$, therefore, the impulse approximation, $\theta = \Delta p / p$, can be used. So, for the deflection angle we have

$$\theta = -\frac{2eq_L}{m\gamma v}\int_{-\infty}^{\infty}\frac{bdt}{b^2 + v^2t^2} = -\frac{2\pi eq_L}{m\gamma v^2}sgn(b). \tag{11}$$

That is the deflection angle received by the electron is actually independent of the impact parameter value *b*.

Let us now try to extend the model to apply to smaller values of the magnitude of the impact parameter b. We must abandon the simple line charge in favor of an X—Y charge distribution $\rho_L(\mathbf{R})$, which is still constant in the Z-direction,

$$\int d^2\mathbf{R}\rho_L(\mathbf{R}) = q_L, \tag{12}$$

where q_L is the X—Y integrated constant linear charge density, as before. In this case, the force on the probe electron is given by the appropriate generalization of Eq.(9),

$$\mathbf{F}(\mathbf{R}) = -2e\int d^2\mathbf{R}'\rho_L(\mathbf{R}')\frac{(\mathbf{R}-\mathbf{R}')}{|\mathbf{R}-\mathbf{R}'|^2}. \tag{13}$$

For the deflection angle we obtain in this case

$$\theta(b) = -\frac{2\pi e}{m\gamma v^2}\int_{-\infty}^{\infty} dY \int_{-\infty}^{\infty} dX\rho_L(X, Y)\, sgn\,(b-X). \tag{14}$$

When the magnitude of the impact parameter b exceeds the X-extent of the charge distribution $\rho_L(X, Y)$, Eq.(14) simply reduces to our previous result given in Eq.(11).

The equation (14) has an interesting property. The only b-dependent factor on the right-hand side of Eq.(14) is $sgn(b-X)$, which appears within the X-integrand. It is well known that differentiating the *sgn* function produces a delta function,

$$\frac{d}{db}\, sgn\,(b-X) = 2\delta(b-X). \tag{15}$$

Thus,

$$\frac{d\theta}{db} = -\frac{4\pi e}{m\gamma v^2}\int_{-\infty}^{\infty} dY\rho_L(b, Y). \tag{16}$$

In other words, the derivative of the deflection angle as a function of impact parameter is proportional to the Y-integrated profile of the transverse beam charge distribution ρ_L. This happens to be precisely the same information as one obtains from a probe wire («flying wire») which is passed perpendicular to the beam in the Y-direction (that of the probe electron) through the X-point corresponding to that electron's impact parameter b.

Figure 19*b* presents the dependence of the X-position of a deflected electron at the detector (at $Y = 2$ cm) *versus* its impact parameter (initial X-position at $Y = -1$ cm). Electrons are «switched» in the X-direction by the proton bunch charge around the center of the proton beam, and the shape of this switching is defined by the proton beam profile.

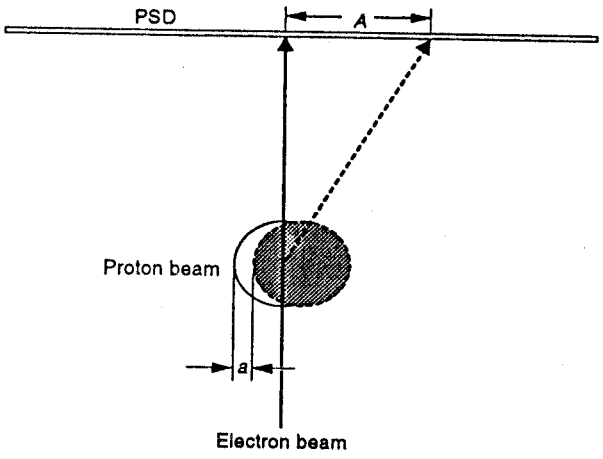

Fig.20. The diagram of the position sensor. 10 KeV electron beam strikes the 20 TeV proton bunch. If the proton bunch is displaced off-center by the distance of a, electron beam position will be displaced by the distance of A. PSD — a position sensitive detector

Our simulation studies for the alternative case with a wide, parallel, uniformly distributed electron beam have shown, that the shape of the beam profile resulting from the interaction with the proton beam is very sensitive to the size of the proton beam [29].

High energy accelerator complexes require feedback systems to dump down injector errors and prevent an emittance growth due to quadrupole vibrations, multibunch instabilities, power supply ripples, etc. Such systems usually involve beam position monitors, providing the information which is used to correct a particle orbit by electrostatic kickers. The noise of a beam position monitor is one of the limiting factors of the systems. An alternative approach to the construction of the essentially «noiseless» beam position monitor based on using a low energy electron beam probe is discussed in paper [31]. Electron beam scattering on an electromagnetic radiation in equilibrium with a temperature of surrounding beam tube is very small and has been neglected.

The diagram of the sensor is presented in Fig.20. If one uses 10 keV electron beam as a probe, the maximum angle of the electron beam deflection by the proton bunch for a collider like the SSC Project is about 40 mrad. Displacement of the bunch with the X-size of 100 μm in transverse direction by the distance of 1 μm typically will cause a deflection of the electron beam by about 0.8 mrad, which at the distance of 50 cm from the 20 TeV beam center translates to about 400 μm, a distance well measurable.

E. Charge Tracing Code for Collider Environment and More Applications. A full Monte Carlo computer code describing behaviour of electrons and ions in the vicinity of any space charges, electrical and magnetic fields was developed. Parameters of the code were optimized for a high energy collider environment. Some results of calculations with a neutral beam profile

monitor, a residual gas beam profile monitor, and an electron beam emittance monitor were published [22].

Transport codes to trace particles in high energy accelerators are well established for many years. However, some miscellaneous processes accompanying acceleration of particles, such as motion of the residual gas ions and electrons in the field of a beam space charge, under the influence of external electrical and magnetic fields usually have not been treated accurately. Nonperturbing beam diagnostics using low energy electron beams as a probe also require special computer codes to understand the results.

The motion of charges in the laboratory frame in some external electrical and magnetic fields and in the presence of some additional moving electrical charges can be described by the equation

$$m\frac{d^2\mathbf{r}}{dt^2} = q(\mathbf{E} + [\mathbf{v}\times\mathbf{B}] + \sum_{i=1}^{n}\mathbf{E}_i + \sum_{i=1}^{n}[\mathbf{v}\times\mathbf{B}_i]) . \qquad (17)$$

Here m is the particle mass, q is its electrical charge, $\mathbf{v}$ — its velocity, $\mathbf{E}$ and $\mathbf{B}$ are external electrical and magnetic fields, $\mathbf{E}_i$ is an electrical field created by the electrical charges nearby the particle (bunch charge), $\mathbf{B}_i$ is a magnetic field associated with a moving charge. In a simulation code a bunch could be presented as a «cloud» of moving electrical charges with a total charge equal to the bunch charge.

The authors [22] found, however, that the practical limit due to a limited speed of computation restricts us to use more than 10^6 separate charge sources in the trajectory code. This amount of charges still does not allow to perform precise trajectory calculations due to the large fluctuations of a «charge density» in such a bunch. This is especially emphasized by the circumstance that the longitudinal size of a bunch at high energy colliders is much larger than its transverse sizes. The design length of the bunch in the collider (the SSC Project case) is of the order of 10 cm, at the same time its transverse sizes are about 100 micrometers. The authors [22] represent the bunch by the set of the «wire» charges. As it happens, it is quite possible to reach a satisfactory solution of the problem with a number of «wire» charges of the order of 10^4. This essentially means that the longitudinal component of the electrical force of the bunch charge is neglected. The code, although being truly three-dimensional, uses a virtually «two-dimensional» X—Y bunch representation. The Z-variation of the bunch charge density is described with the corresponding time variation of the «wire» charge (and current) density. Lorentz shrinking of the electrical field of an individual proton does not really change the time integral of the bunch field in the case of the dense bunch [32].

The *X*- and *Y*-distributions of the bunch charge were varied separately according to the desired shape — Gaussian, uniform density, etc. The electromagnetic field created by each «wire» is calculated as a field of infinitely long wire with a charge (and a current) density variable in the *Z*-direction:

$$\mathbf{E}_i = \frac{q_i(Z)\mathbf{u}_r}{2\pi\varepsilon_0 r}, \tag{18}$$

$$\mathbf{B}_i = \frac{1}{c^2}(\mathbf{v} \times \mathbf{E}_i). \tag{19}$$

In its turn, $Z = Z(t) = ct$, c is a speed of light, $\mathbf{v}$ is a bunch velocity. Additional input parameters are ion (or electron) velocity and magnitudes of the external electrical and magnetic fields.

Tracking a particle in ZBEAM code is achieved by integrating the equation of motion over successive small time steps. Tracking stops when the particle reaches a detector or leaves the region of interaction.

ZBEAM code was used for calculations of possible beam-beam space charge effect compensation in colliders, described earlier. Low energy electron probe monitor calculations described earlier are based also on this code. In addition, a residual gas ionization beam profile monitor for the SSC was considered in detail [33] using ZBEAM code [22]. It was shown that a good spatial resolution in beam profile measurements could be obtained using a combination of electrical and magnetic fields.

Calculations indicate that the statistics are high enough to expect good spatial resolution for a residual gas ionization monitor. However, systematic effects could smear the resolution for the SSC beam. Electrons produced with velocity close to zero are affected by beam charge, and so the space information could be essentially lost. One can expect a better performance of such a monitor if strong external electrical and magnetic fields are applied.

A diagram of the residual gas ionization monitor using a dipole magnetic field is presented in Fig.21. Two magnets are used to compensate for the influence of the magnetic field on beam dynamics. Electrons are accelerated up to the energy of about 30 keV and detected by a position sensitive detector. One can achieve some magnification of the beam profile image using specially shaped magnetic and electrical fields.

A two-dimensional Gaussian distribution with $\sigma_x = \sigma_y = 50$ μm was used to describe a bunched beam; the bunch length was taken to equal 10 cm, and protons were uniformly distributed in the *Z*-direction. The number of protons in the bunch was 10^{10}. External electrical and magnetic fields directed along the *Y*-axis (perpendicular to the beam direction) were applied. Ion-electron pairs are produced in space according to the proton density in a bunch. The energy

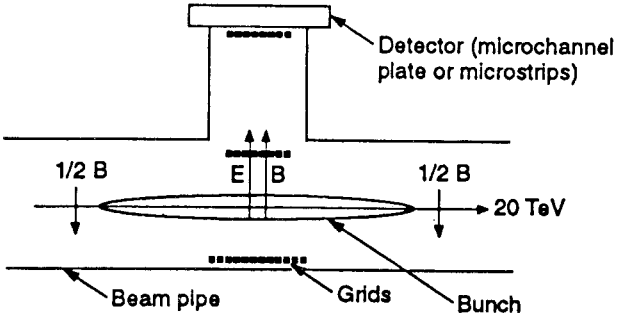

Fig.21. Residual Gas Ionization Beam Profile Monitor for the SSC

spectrum of electrons was produced according to a $1/E^2$ dependence, beginning from $E_e = 3$ eV. It was assumed that 90% of electrons will produce a good image of the beam, i.e., the authors neglect 10% of all electrons with recoil energy of more than 30 eV. The velocity vectors of the electrons were distributed isotropically in space. Finally, electrons were «collected» by the detector at the $Y = 2$ cm plane.

The distribution of electrons arriving at the detector plane of the residual gas ionization monitor for a uniform magnetic field of 2 T and external constant electrical field of 10 kV/cm was studied. An rms spread of about 5 μm was obtained, and this was satisfactory for the requirements to the SSC emittance monitors.

SUMMARY

As was already mentioned, beam extraction experiments with bent crystals are in progress at CERN and Fermilab. 10^7 protons per spill are being extracted on a regular basis from the 70 GeV accelerator at IHEP, Serpukhov. Studies related to the crystal extraction from the LHC are planned at CERN. However, rather low extraction efficiencies (about 10% at CERN SPS) up to now have been a serious obstacle to a practical use of the method. The studies [8] promise to overcome this limitation and open the way for wider application of the technique.

During these studies the authors believe they found the practical way to make proton collider a double feature machine, producing low intensity extracted beams simultaneously with colliding beam experiments. They have presented a high efficiency stationary passive device for the beam halo crystal

extraction. It would extract the natural proton beam loss, the beam halo, which for the Tevatron is about 2×10^7 protons per second, and about 10^9 protons per second for the LHC. The process does not interfere with colliding beam experiments. Thus, the device is suitable for cleaning up the proton beam halo (a clean crystal scraper), or for useful extraction of the proton beam halo particles with about a 99% efficiency. When it is used as a clean scraper, it could work as an efficient clean radiation drain preventing radiation due to a proton beam loss. Alternatively, small fixed target experiments could be carried out making use of this proton flux, including fixed-target B physics. The device could enhance detector R&D studies.

The device is suitable to be used at the LHC collider for both circulating proton beams. It could reduce the background radiation due to a beam halo loss by a factor of about 100.

Computer simulations were carried out to study the decoherence of beam oscillations in the SSC in head-on beam-beam interactions in a collider. It was found that, for the SSC baseline conditions, the decoherence time due to the beam-beam tune spread would be around 0.1 second, about seven times shorter than the previous theoretical estimate. Since the damping time should be short compared with the decoherence time, this result has important consequences for the design of the damping systems.

It was shown that the head-on beam-beam effect in proton-proton machines might be compensated, under appropriate conditions, by collisions of the bunch on each turn with a space charge of the opposite sign. For the positively-charged proton beams, for example, such an opposite-sign space charge might be provided by a low energy electron beam. Studies carried out for the SSC Project and for the LHC indicate that for reasonable tolerances on the electron beam parameters it is possible to achieve a good beam-beam effect compensation and reduce a tune spread due to the head-on space charge beam-beam effect by two orders of magnitude, which would improve considerably the high-luminosity performance of future colliders.

A full Monte Carlo computer code describing the behavior of electrons and ions in the vicinity of a space charge, and of electrical and magnetic fields was developed. The parameters of the code were optimized for a collider environment. Calculations were performed with the code for a residual-gas beam profile monitor, and an electron-beam-probe emittance monitor.

Initially the use of flying wires and synchrotron radiation imaging were proposed for determining the beam profile for the SSC Project. It was thought that the synchrotron radiation imaging would provide a continuous, non-interfering monitor of the beam profile. However, closer examination revealed that, because of a small size and high energy of the beam, the image would suffer from a large amount of diffraction broadening. This broadening would

reduce the sensitivity of the measurement to an unacceptable level. The realization of this difficulty led to a survey of the known minimal-interference measurement techniques which might be applicable at the SSC for determining the beam size. It was concluded that, of the approaches that appeared to be feasible, use of a low-energy electron beam probe offered the most promise. The results of simulations using this approach showed promise for providing useful transverse and longitudinal beam profile measurements, and this could be effectively used at the LHC.

In the course of the SSC Project design the authors [24] devised and studied a so-called «intelligent» damping scheme, involving the use of two kickers, spaced by preferably 1/4 betatron wave lengths. This design provides the capability of exactly canceling the coherent betatron oscillations for each bunch in a single turn, in contrast to the statistical cancellation of previous devices. The cancellation would be independent of betatron oscillation phase. This scheme would be vital for the LHC and future colliders because of the very strict operational tolerances required.

ACKNOWLEDGEMENTS

The authors wish to thank Drs. S.Baker, G.Bourianoff, R.Carrigan, A.Chao, T.Dombeck, G.Dugan, D.Edwards, H.Edwards, D.Green, G.Jackson, D.Johnson, S.Kauffmann, D.Larson, G.Lopez, R.Meinke, G.Mitselmakher, N.Mokhov, T.Murphy, W.Nexsen, W.K.H.Panofsky, J.Peoples, R.Richardson, G.Seaborg, H.-J.Shih, N.Slavin, G.Stupakov, R.Talman, M.Tigner, A.Tollestrup, T.Toohig, and G.Trilling for their valuable help and discussions. The authors express their gratitude to the CERN SL/AP Division for the hospitality during the studies. Support of Prof. A.Baldin during these studies is very appreciated.

REFERENCES

1. **Tsyganov E.** — Some Aspects of the Mechanism of a Charge Particle Penetration Through a Monocrystal, Fermilab TM-682, Batavia (1976); **Elishev A. F. et al.** — Phys. Lett., 1979, B 88, p.387; **Carrigan R. A. et al.** — Nucl. Instrum. Methods, 1982, 194, p.205.
2. **Avdeichikov V. V. et al.** — JINR Rapid Communications, 1984, 1-84, p.3, English translation FERMILAB-FN-429, February 1986.
3. **Asseev A.A. et al.** — Proceedings of 1991 Particle Accelerator Conference, p. 189, May 1991, San Francisco, CA; **Asseev A. A. et al.** — IHEP Preprint 89-57, Serpukhov, 1989.
4. **Akbari H. et al.** — Phys. Lett., 1993, B313, p.491.

5. **Carrigan R. A. et al.** — Proposal for a Test of Low Intensity Extraction From the Tevatron Using Channeling in a Bent Crystal, FNAL, May 22, 1991; **Jackson G.** — In: Proceedings of the 1993 Particle Accelerator Conference, p. 1366, Washington, May 1993; **Carrigan, R. A. Jr., et al.** — Nucl. Instrum. Methods, 1994, B 90, p.128; **Murphy T.** — Invited talk "Bent Crystal Beam Extraction from Tevatron", Aarhus Workshop on Relativistic Channeling, July 1995.
6. **Newberger B. S. et al.** — Nucl. Instrum. Methods, 1993, A325, p.9; **Gabella W. et al.** — In: Proceedings of the 1993 Particle Accelerator Conference p. 233, Washington, May 1993.
7. **Tsyganov E., Shih H.-J., Taratin A.** — Resonance Excitation of the SSC Beam Halo by RF Voltage Pulses, SSCL-609, December 1992.
8. **Tsyganov E., Taratin A.** — Nucl.Instrum.Methods, 1995, A 363, p.511.
9. **Taratin A., Tsyganov E.** — presented at Fermilab AD seminar, September 12, 1994.
10. **Mokhov N.** — «Scrapers», private communication.
11. **Finley D.A.** — In: Proceedings of the 1993 Particle Accelerator Conference, p. 3721, Washington, May 1993.
12. **Jackson G.** — In: Proceedings of the 1993 Particle Accelerator Conference, p. 402, Washington, May 1993.
13. **Baker S.I.** — Radiation Damage Effects in Channeling Applications, in Relativistic Channeling, edited by R. Carrigan, Jr., and J. Ellison, Plenum Press, New York and London, 1987, p. 391; **Chesnokov Yu.A. et al.** — In: Proc. 15th Int. Conf. on High Energy Accelerators, 1992, Int. J. Mod. Phys. A (Proc. Suppl.), 1993, 2, p.173; **Baker S.I. et al.** — Nucl.Instrum.Methods, 1994, B 90, p.119.
14. **Taratin A. et al.** — Ultrathin Crystal Scatterer for the SSC Beam Extraction System, SSCL-545, December 1991.
15. **Taratin A.M. et al.** — Nucl. Instrum. Methods, 1990, B47, p.247.
16. **Shih H.-J., Taratin A.** — Bent Crystal Extraction of the SSC Beam with RF Noise Induced Diffusion, SSCL-389, March 1991.
17. **Tsyganov E., Shih H.-J., Meinke R., Nexsen W., Herath-Banda M., Taratin A.** — SSCL-Preprint-481, July 1993, submitted to IEEE NS.
18. **Lebedev V.A., Parkhomchuk V.V., Shiltsev V.D., Skrinsky A.N.** — INP Preprint 91-120, Novosibirsk, 1991; **Lebedev V.A.** — SSCL-Preprint-191, March 1993.
19. **Evans L.R.** — In: CERN Accelerator School on Antiprotons for Colliding Beam Facilities, CERN Report 84-15, p.319, 1984.
20. **Stupakov G.V., Parkhomchuk V.V., Shiltsev V.D.** — SSCL-Preprint-495, August 1993.
21. **Tsyganov E., Meinke R., Nexsen W., Zinchenko A.** — SSCL-Preprint-519, October 1993.
22. **Tsyganov E., Zinchenko A.** — SSCL-618, March 1993.
23. **Tsyganov E., Taratin A., Zinchenko A.** — Beam-Beam Effect Compensation at the LHC, CERN SL/Note 95-116 (AP).
24. **Tsyganov E., Dugan G., Lopez G., Meinke R., Nexsen W., Talman R.** — IEEE NS, v. 41, p. 287, 1994.
25. **Penner S.** — SSCL Internal Note, July 18, 1991.
26. **Chen S., Lopez G.** — Simulation Studies of the Transverse Dipole Mode Multibunch Instability for the SSC Collider, SSCL-614, 1993.

27. **Galayda J.** — In: American Institute of Physics Conference Proceedings 249, Physics of Particle Accelerators, M. Month and M. Dienes, Editors, New York, 1991, v. 1, p.663.
28. **Zhabitsky V.M.** — JINR P9-91, Dubna, 1991 (in Russian).
29. **Tsyganov E., Meinke R., Nexsen W., Kauffmann S., Zinchenko A., Taratin A.** — SSCL-Preprint-179, December 1992, Published in Proc. 1993 PAC, Washington, D.C., May 1993, p. 2489.
30. **Pasour J., Ngo M.** — Rev. Sci. Instrum. 63 (1992) 3027.
31. **Tsyganov E., Kauffmann S., Meinke R., Nexsen W., Richardson R.** — SSCL-619, March 1993.
32. **Jackson J.D.** — Classical Electrodynamics, Wiley, New York, 1962.
33. **Meinke R., Nexsen W., Tsyganov E., Zinchenko A.** — SSCL-Preprint-353, May 1993, Published in Proc. 1993 PAC, Washington, D.C., May 1993, p. 2468.